TIME RESOLVED ELECTROPHORETIC AND ELECTROOSMOTIC VELOCITIES

By

RAVI GHANSHYAM PATEL

A thesis submitted to the

Graduate School-New Brunswick

Rutgers, The State University of New Jersey

In partial fulfillment of the requirements

For the degree of

Master of Science

Graduate Program in Mechanical and Aerospace Engineering

Written under the direction of

Professor Francisco Javier Diez

And approved by

_____

_____

_____

New Brunswick, New Jersey

October 2013

ABSTRACT OF THE THESIS

Time Resolved Electrophoretic and Electroosmotic Velocities

By RAVI GHANSHYAM PATEL

Thesis Director:
Professor Francisco Javier Diez

Electroosmotic pumps show promise in many fields. For example, several lab-on-chip devices have been proposed the make use of these devices [(1)]. This thesis will focus on finding the fluid velocity distribution inside an electroosmotic pump. First, the fluid velocity was calculated for an electroosmotic pump using a bipolar pulse train voltage. Next, the particle velocity for particles suspended in the fluid was found. A glass electroosmotic pump was constructed using a glass capillary tube. Using a 1mM Borate buffer solution and 0.5μm Fluosphere particles, time resolved micro particle image velocimetry (TRμPIV) was performed on the pump to obtain the particle velocity distribution inside the pump. The experiment fluid velocity was calculated from this particle velocity. The experimental particle and fluid velocities show excellent agreement with the theoretical calculations.

Acknowledgements

I would first like to thank my advisor Professor Diez for his advice and guidance during my graduate studies.

I would also like to thank Professors Shan and Bagchi for taking the time to review my thesis and participating on my committee.

I would like to thank everyone in Professor Diez's lab. Thank you for taking the time to help me and for all of your advice.

Finally, I would like to thank my family and friends for their encouragement and support.

Table of Contents

Title i

Abstract ii

Acknowledgements iii

Table of Contents iv

List of Symbols vi

Variables and Constants vi

Subscripts and Superscripts viii

List of Figures ix

Chapter 1 1

1.1. Introduction 1

1.2. Electroosmosis and Electrophoresis 1

1.3. Thesis Outline 7

Chapter 2 11

2.1. Derivation of flow and flow rate using Duhammel's theorem and separation of variables 11

2.2. Derivation of steady state flow rate 14

2.3. Movement of Particles due to Electrophoresis and Electroosmosis 19

Chapter 3 29

3.1. Manufacturing 29

3.2. Cleaning and Preparation 30

3.3. Experimental Procedure 31

Chapter 4 35

4.1. Finding the parameters 35

4.2. Particle velocity due to bipolar pulse train voltage 36

Conclusion 46

References 47

List of Symbols

Variables and Constants

ψ	Gradient of the electrostatic potential
$\boldsymbol{r}$	Position vector
x	Widthwise coordinate
y	Heightwise coordinate
z	Lengthwise coordinate
ε	Dielectric constant
n_i	Ion concentration
e	Faraday Constant
z_i	Ion charge
k	Boltzmann constant
T	Temperature
κ^{-1}	Debye length
ζ	Zeta potential
P	Pressure
$\boldsymbol{u}$	Velocity
$\boldsymbol{f_e}$	Coulomb force
ν	Viscosity
μ	Dynamic viscosity
$\boldsymbol{E}$	Electric field

μ_{eo}	Electroosmotic mobility
μ_{ep}	Electrophoretic mobility
τ	Time constant
ρ	Density
d_p	Diameter of the particles
t	Time
u	Velocity
V	Voltage
u^+	Electroosmotic velocity generated by V^+
u^-	Electroosmotic velocity generated by V^-
t^+	Length of positive voltage pulse
t^-	Length of negative voltage pulse
h	Channel height
w	Channel width
u_{slip}	Electroosmotic slip velocity
Φ	Fluid velocity step response
Ψ	Flow rate step response
$g^+(\tau_j) - g^-(\tau_j)$	Magnitude of step change
H	Heaviside step function
Ψ	Particle velocity
β_m	mth eigenvalue
$\tau_{1,n}$	Location of nth positive to negative voltage transition

$\tau_{2,n}$	Location of nth negative to postive transition
Q	Flow rate
Q_{avg}	Average flow rate
$F_{ep}(t)$	Electrophoretic force
f_{ep}	Electrophoretic force per unit particle mass

Subscripts and Superscripts

$+$	Associated with positive voltage pulse
$-$	Associated with negative voltage pulse
o	Associated with applied voltage
w	Wall
p	Particle
f	Fluid
ep	Electrophoretic
eo	Electroosmotic
avg	Average

List of Figures

Figure 1.1. Diagram of the double layer according to the Gouy-Chapman-Stern model ... 9

Figure 1.2. Diagram of the electrophoretic and electroosmotic effects ... 10

Figure 2.1. Bipolar pulse train waveform. ... 23

Figure 2.2. Geometry of microchannel ... 24

Figure 2.3. Instantaneous flow velocity for 1Hz waveform. ... 25

Figure 2.4. Instantaneous flow velocity for 100Hz waveform. ... 26

Figure 2.5. Comparison of steady state and transient flow rates ... 27

Figure 2.6. Effect of duty cycle on average flow rate. ... 28

Figure 3.1. Electroosmotic pump used in experiments ... 33

Figure 3.2. Diagram of experimental set up ... 34

Figure 4.1. Particle velocity using a step waveform ... 39

Figure 4.2. Selected velocity profiles using a square waveform ... 40

Figure 4.3. Particle velocity due to a $200V_{p-p}$, 100Hz square waveform ... 42

Figure 4.4. Fluid velocity due to a $200V_{p-p}$, 100Hz square waveform ... 43

Figure 4.5. Comparison of flow rate vs. time using a square waveform. ... 44

Figure 4.6. Comparison of flow rate vs. time using a bipolar pulse train ... 45

Chapter 1

1.1. Introduction

Electrokinetics is the study of phenomena that occur due to boundary interactions between solids and fluids. This thesis focus of two kinds of these phenomena: electroosmosis and electrophoresis. Electroosmosis is the motion of fluid near a solid wall due to the presence of an electric field. Electrophoresis is the motion of particles in a fluid due to the presence of an electric field.

Electrokinetic phenomena have many useful applications, particularly in microfluidics. For example, using the electroosmotic effect, it is possible to construct a micro pump with no moving mechanical parts. In addition, the electrophoretic effect can be used to separate particles suspended in solution [(2)]. This enables upcoming technology such as lab-on-chip [(1)]. This thesis will focus on the movement of particles inside an electroosmotic pump. The fluid and particle velocities will be found theoretically and experimentally and compared.

1.2. Electroosmosis and Electrophoresis

When a fluid comes in contact with a solid, ions in the fluid organize to form an electric double layer next to the solid wall . The layer adjacent to the wall is formed by chemical interactions between the fluid and the solid. Its potential attracts the second layer by the Coulomb force. The Gouy-Chapman-Stern model is often used to describe the double layer (see Figure 1.1). This model assumes that ions in the first layer, called the Stern layer, are stationary with respect to the surface of the solid and the ions in the

second layer, called diffuse layer, move freely. In electroosmosis double layer forms on the surface is the wall in contact with the fluid. In electrophoresis the double layer forms around the surface of the particle suspended in the fluid [3]. Figure 1.2 shows a diagram of the electroosmotic and electrophoretic effects.

Past the Stern layer, charge is assumed to be distributed according to the Poisson-Boltzmann equation [4]:

$$\nabla^2\psi(\boldsymbol{r}) = -\frac{1}{\varepsilon}\sum_{i=1}^{m} n_i\, ez_i \exp\left(-\frac{ez_i}{kT}\psi(\boldsymbol{r})\right) \qquad (1.1)$$

Where ψ is the electric potential at $\boldsymbol{r}$ due to the double layer, ε is the permittivity of the fluid, the summation is over each ion in the fluid, n_i is the concentration of the ion in the bulk fluid, *e* is the Faraday Constant, z_i is the charge of the ion, k is the Boltzmann constant, and T is the temperature. Because this equation is nonlinear, solutions exist for only a few special cases. Therefore, this equation is often simplified by assuming symmetric electrolytes, where ion and counter ion have the same charge. In one dimensional rectangular coordinates [2]:

$$\frac{\mathrm{d}^2\psi(y)}{dy^2} = \frac{2nez}{\varepsilon}\sinh\left(\frac{ez}{kT}\psi(y)\right) \qquad (1.2)$$

The equation is often linearized by using the Debye-Huckel approximation, when $\frac{ez_i}{kT}\psi$ is small [5]:

$$\frac{\mathrm{d}^2\psi(y)}{dy^2} = \frac{2ne^2z^2}{\varepsilon kT}\psi(y) \qquad (1.3)$$

The Debye length, $\kappa^{-1} = \left(\frac{\varepsilon kT}{2ne^2z^2}\right)^{1/2}$, characterizes the length at which the potential decays. This equation can be solved using a boundary condition. However, there is some uncertainty as to what boundary condition to use. The potentials at the Stern layer

and through the diffuse layer are estimated to be very high, but cannot be measured using current techniques. It is common to use the potential at the shear plane, where the no slip condition can be applied, because it is possible to experimentally determine the potential here. The potential at the shear plane is called the zeta potential [4]. Equation 1.3 is integrated on the semi-infinite domain, defining $y = 0$ at the shear plane, to find:

$$\psi = \zeta e^{-\kappa y} \qquad (1.4)$$

At the solid-liquid interface, the material of the solid and the composition of the liquid determine the chemical interactions in the Stern layer, and so they determine the zeta potential. The chemical interactions in the solid-liquid interface, however, are very complex, so the zeta potential cannot be derived theoretically [5]. From experiments, the surface material and roughness, the solutes and solvent, the pH of the solution, and the concentration of solution all significantly affect the zeta potential. Extremely dilute solutions do not follow the thin double layer approximation. The zeta potential cannot be measured directly because of the small scale of the double layer and techniques used to find the zeta potential rely on indirect measurements.

Electroosmosis causes fluid in contact with a surface to flow under an electric field. In an electroosmostic flow, an electric field is applied tangentially to a surface. The ions in the diffuse layer move according the Coulomb force generated by the electric field. They drag the surrounding fluid, which in turn viscously drags the bulk fluid. The motion of charged fluid above a fixed flat plate due to an electric field is used to represent electroosmosis. Similarly, in electrophoresis, the electric field creates a force on the ions in the Stern layer which transfers to the particle. A coordinate transform is used so that the particle is represented by a mobile flat plate [2]. The motion of the charged

fluid above this plate due to an electric is used to represent electrophoresis. The velocity generated by electroosmosis, on the fluid, or electrophoresis, on the particle, can be used to find the zeta potential. This velocity can be calculated using the Navier-Stokes equation in conjunction with the potential distribution as shown above in Equation 1.4 (2).

$$\frac{D\boldsymbol{u}(\boldsymbol{r})}{Dt} = -\frac{\nabla P(\boldsymbol{r})}{\rho} + \nu\nabla^2\boldsymbol{u}(\boldsymbol{r}) + \boldsymbol{f_e}(\boldsymbol{r}) \qquad (1.5)$$

Where $\boldsymbol{u}$ is the flow velocity, P is the pressure, ρ is the density of the fluid, ν is the kinematic viscosity, and $\boldsymbol{f_e}$ is the Coulomb force caused by the electric field. According to the Poisson Equation, the Coulomb force can be written as

$$\boldsymbol{f_e}(\boldsymbol{r}) = \rho_e(\boldsymbol{r})\boldsymbol{E}(\boldsymbol{r}) = -\varepsilon\boldsymbol{E}(\boldsymbol{r})\nabla^2\psi(\boldsymbol{r}) \qquad (1.6)$$

Where $\rho_e$is the charge density of the fluid and $\boldsymbol{E}$ is the applied electric field. Microfluidic flows are relatively slow moving and have small characteristic lengths, so the Reynolds numbers are small, and Stokes flow can be used as an approximation. In addition, pressure gradients can be ignored. The zeta potential is assumed to be a physical property that does not depend on time, so the flow can be taken to be steady. The electric field is assumed to be unidirectional, uniform, and applied in the lengthwise direction. For one dimensional rectangular coordinates and uniform electric field, the equation reduces to [(4)]:

$$\frac{d^2u(y)}{dy^2} = \frac{\varepsilon E}{\nu}\frac{d^2\psi(y)}{dy^2} \qquad (1.7)$$

For electroosmosis, this equation is integrated using the semi-infinite domain boundary conditions: ($u(y=0) = 0$ and $\left.\frac{du}{dy}\right|_{y\to\infty} = 0$ (where y=0 at the shear plane) to give:

$$u_{eo}(y) = \frac{\varepsilon E \zeta_w}{\nu}(e^{-\kappa y} - 1) \quad (1.8)$$

u_{eo} and ζ_w have replaced u and ζ to represent the electroosmotic velocity and wall zeta potential, respectively. The potential, ψ, is approximated using Debye Huckel approximation (see Equation 1.4). For small Debye lengths ($\kappa y \gg 1$), the exponential term vanishes and the electroosmotic velocity becomes [2]:

$$u_{eo} = -\frac{\varepsilon \zeta_w}{\nu} E \quad (1.9)$$

For electrophoresis, Equation 1.7 is integrated using the semi-infinite domain boundary conditions: ($u(y = 0) = \frac{\varepsilon E \zeta}{\nu}$ and $u|_{y \to \infty} = 0$ (where y=0 at the shear plane) to give:

$$u_{ep}(y) = \frac{\varepsilon E \zeta_p}{\nu}(e^{-\kappa y}) \quad (1.10)$$

u_{ep} and ζ_p have replaced u and ζ to represent the electrophoretic velocity and particle zeta potential, respectively. The potential, ψ, is approximated using Debye Huckel approximation (see Equation 1.4). The velocity of the particle is the velocity at the wall.

$$u_{ep} = \frac{\varepsilon \zeta_p}{\nu} E \quad (1.11)$$

For convenience, Equations 1.9 and 1.11 are written as follows [2]:

$$u_{eo} = \mu_{eo} E, \text{ where } \mu_{eo} = -\frac{\varepsilon \zeta_w}{\nu} \quad (1.12)$$

$$u_{ep} = \mu_{ep} E, \text{ where } \mu_{ep} = \frac{\varepsilon \zeta_p}{\nu} \quad (1.13)$$

μ_{eo} and μ_{ep} are defined as the electroosmotic and electrophoretic mobilities. They are properties of the solid-liquid interface and do not depend on the electric field. Equations 1.12 and 1.13 are known as the Smoluchowski equation [2].

Through these calculations, the fluid velocity produced by electroosmosis and the particle velocity produced by electrophoresis are shown to be directly proportional to the zeta potential. This demonstrates the importance of measuring the zeta potential for electroosmosis and electrophoresis. Techniques used to measure the zeta potential by electroosmosis consist of finding the electroosmotic velocity so that the zeta potential can be calculated by Equation 1.9 and 1.11. From this, it is clear why the zeta potential is defined as the potential at the shear plane. Fluid flow does not occur between the surface and the shear plane, so the electroosmotic mobility is only affected by the flow velocity of the fluid which is viscously dragged to the velocity in Equation 1.12 and 1.13 by the shear layer.

If the walls and particles are far enough apart, the double layers do not overlap and the Poisson-Boltzmann equation holds. The Debye-Huckel approximation can then be applied if the zeta potential can be assumed to be small. The thin double layer approximation can be used if the Debye length is small. As long as these conditions are satisfied, an experimentalist can calculate the zeta potential from Equations 1.12 and 1.13 by finding the velocities of the particles or fluid under an applied electric field. Using this zeta potential, the velocity of the particles and fluid can be predicted for other electric fields.

Minor [6] [7] has shown that the characteristic response time for the electroosmotic and electrophoretic effect are:

$$\tau_{eo} = O\left(\frac{4h^2\rho_w}{\mu}\right) \tag{1.14}$$

$$\tau_{ep} = O\left(\frac{d_p^2\rho_w}{\mu}\right) \tag{1.15}$$

The electrophoretic effect occurs at a much faster time scale than the electroosmotic effect because the diameter of the particles are much smaller than the height of the microchannel.

1.3. Thesis Outline

The electroosmotic and electrophoretic effect can be generated inside a fluid filled microchannel under an applied electric field. Each wall acts as the solid-liquid interface for electroosmosis. Particles can be added to the microchannel. Under the applied electric field, electroosmosis would drive the fluid and electrophoresis would drive the particles. The pressure from the fluid would also create a force on the particles.

In this thesis the movement of particles inside an electroosmotic channel will be measured, so both electrophoresis and electroosmosis are considered. In the previous section, the electroosmotic velocity was found. However, if the electric field is applied at a high enough frequency the fluid velocity would never fully develop. It must be considered unsteady and varying throughout the cross section of the channel. The fluid is driven by electroosmosis and the particles are viscously dragged by the fluid as well as by the electrophoretic force. This particle velocity is solved for. The electrophoretic effect is assumed to take effect instantly after voltage is applied because it acts on a much faster time scale. An electroosmotic pump is constructed and filled with a particle mixture. As power is applied to the channel, the velocity of the particles is measured

using time resolved micro particle image velocimetry (TRμPIV) [7] [8]. This experimental velocity is compared to the derived velocity.

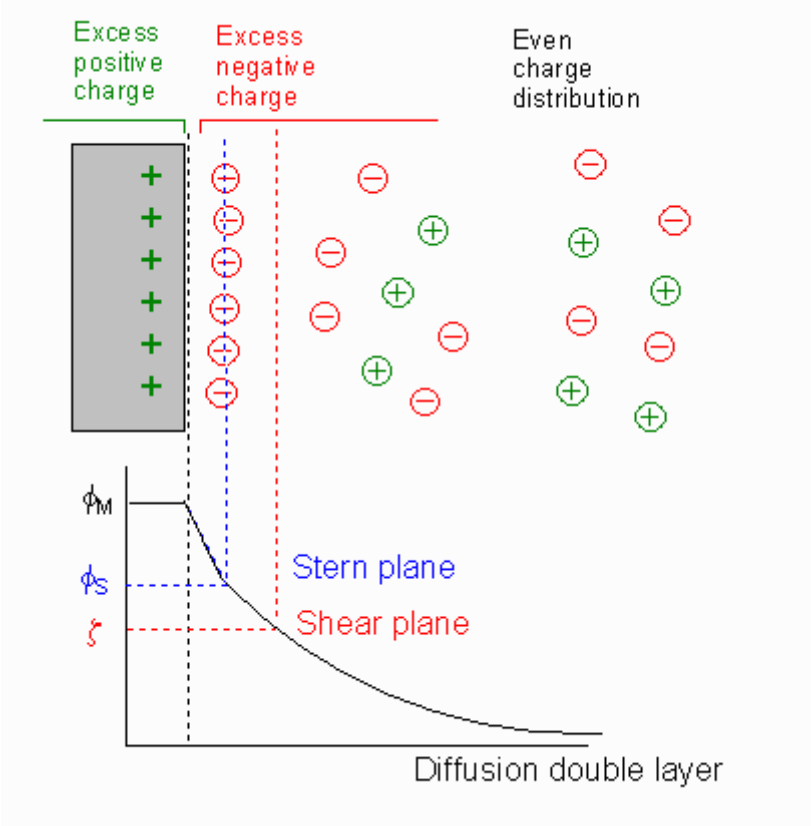

Figure 1.1. Diagram of the double layer according to the Gouy-Chapman-Stern model [9]

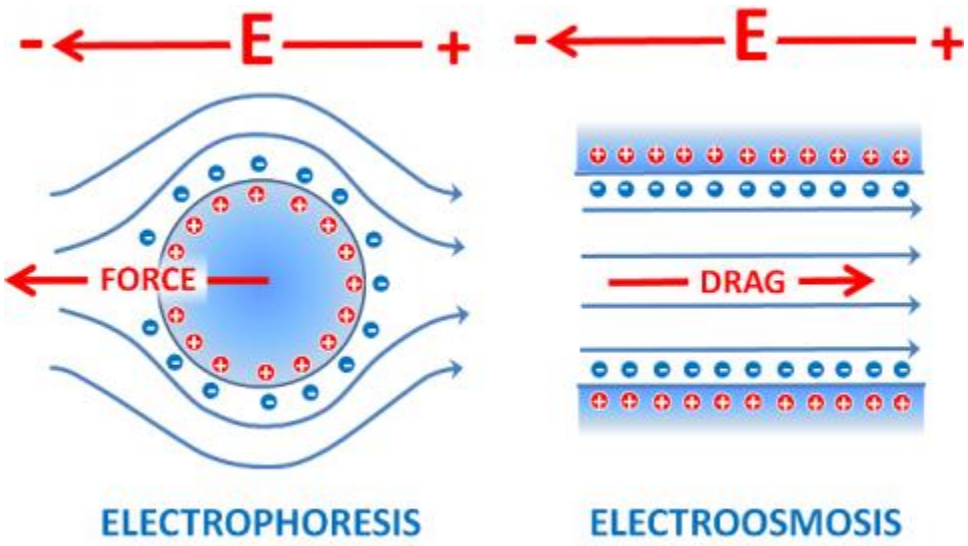

Figure 1.2. Diagram of the electrophoretic (left) and electroosmotic (right) effects. The double layers at the solid-liquid interface react to the electric field and cause a force on the particle (left) and the fluid (right).

Chapter 2

2.1. Derivation of flow and flow rate using Duhammel's theorem and separation of variables

The flow profile generated by applying a time dependent voltage is modeled here using a variation of Stokes' First and Second Problem. Electroosmotic flows typically have very low Reynolds numbers, so they can be assumed to be Stokes flows. The diffuse layer can be represented as the plate in Stokes' Second Problem [10], moving at a velocity equal to the electroosmotic slip velocity. The velocity is assumed to be linear with the applied voltage. This is approximately true because the response time for the electroosmotic slip velocity is very fast. The electric field is applied as a bipolar pulse train waveform as shown in Figure 2.1. Therefore, according to Equation 1.12, the slip velocity is assumed to be the same function scaled by the electroosmotic mobility. u^+ is defined as the electroosmotic velocity associated with the positive voltage pulse and u^- is electroosmotic velocity associated with the negative voltage pulse.

Figure 2.2 shows the geometry of the channel. Assuming the width of the channel is large compared to the height of the channel, the electroosmotic effects due to the side walls can be neglected and the problem can be modeled as the fluid flow between two infinite plates moving at the electroosmotic slip velocity.

As in Stokes' Problems, the governing equation is the diffusion equation [11]. However, in Stokes' Second Problem, u_{slip} would have a simple sinusoidal expression, but in this problem, the velocity follows the same curve as the voltage, multiplied by a scaling factor. The velocity initially is taken to be zero for all y. By symmetry, the top half and bottom half the channel are identical, so only the top half the channel needs to be

solved for, using the symmetry boundary condition at the center of the channel. The electroosmotic slip velocity is used as the boundary condition for the top of the channel. The fluid velocity profile $u_f(y,t)$ can be found from the follow PDE:

$$\begin{gathered} \frac{\partial u_f}{\partial t} = \nu \frac{\partial^2 u_f}{\partial y^2} \\ u_f(h,t) = u_{slip} = g(t) \\ \left.\frac{\partial u_f}{\partial y}\right|_{y=0} = 0 \\ u_f(y,0) = 0 \end{gathered} \tag{2.1}$$

By Duhamel's Theorem [12] [13], the solution to the above problem is:

$$\begin{aligned} u_f(y,t) = &\int_0^t \Phi(y,t-\tau)\frac{\partial g(\tau)}{\partial \tau}d\tau \\ &+ \sum_{j=0}^{\infty} \Phi\left(y,t-\tau_j\right)\left(g^+\left(\tau_j\right) - g^-\left(\tau_j\right)\right)d\tau \end{aligned} \tag{2.2}$$

Since $g(t)$ is a bimodal pulse train, it is composed of a series of discontinuities. $g^+\left(\tau_j\right) - g^-\left(\tau_j\right)$ is the difference in $g(t)$ at the discontinuity $t = \tau_j$. $\Phi(y,t)$ is the solution to the following homogeneous PDE:

$$\begin{gathered} \frac{\partial \Phi}{\partial t} = \nu \frac{\partial^2 \Phi}{\partial y^2} \\ \Phi(h,t) = 1 \\ \left.\frac{\partial \Phi}{\partial y}\right|_{y=0} = 0 \\ \Phi(y,0) = 0 \end{gathered} \tag{2.3}$$

$\Phi(y,t)$ can be solved for using separation of variables [13]:

$$\Phi(y,t) = 1 + \frac{2}{h}\sum_{m=1}^{\infty} \frac{(-1)^m}{\beta_m}\cos(\beta_m y)\, e^{-\nu\beta_m^2 t} \tag{2.4}$$

Where β_m is $\frac{(2m-1)\pi}{2h}$. The discontinuities in f(t) occur at:

$$\begin{matrix} n(t^+ + t^-) : n = 1,2, \dots \\ (n-1)(t^+ + t^-) + t^+ : n = 1,2, \dots \end{matrix} \quad (2.5)$$

At the first set of discontinuities, the expression $g^+(\tau_j) - g^-(\tau_j) = -u^+ + u^-$ and at the second set, the expression $g^+(\tau_j) - g^-(\tau_j) = u^+ - u^-$. From Duhamel's equation, the final solution is [12] [13]:

$$u_f(y,t) = u^+\Phi(y,t) + (u^+ - u^-)\sum_{n=1}^{\infty}(\Phi(y, t-\tau_{1,n})H(t-\tau_{1,n}) - \Phi(y, t-\tau_{2,n})H(t-\tau_{2,n})) \quad (2.6)$$

Where $\tau_{1,n} = n(t^+ + t^-)$, $\tau_{2,n} = (n-1)(t^+ + t^-) + t^+$, and $H(t-\tau)$ is the Heaviside step function. The volume flow rate, Q, is calculated by integrating over the cross sectional area of the channel:

$$Q(t) = 2\int_0^h \int_0^w u(y,t)dxdy \quad (2.7)$$

This evaluates to:

$$Q(t) = u^+\Psi(t) + (u^+ - u^-)\sum_{n=1}^{\infty}(\Psi(t-\tau_{1,n})H(t-\tau_{1,n}) - \Psi(t-\tau_{2,n})H(t-\tau_{2,n})) \quad (2.8)$$

Where:

$$\Psi = 2w\left(h + \frac{2}{h}\sum_{m=1}^{\infty}\frac{(-1)^m \sin(\beta_m h)}{\beta_m^2}e^{-\nu\beta_m^2 t}\right) \quad (2.9)$$

$\Phi(y, t-\tau_{1,n})H(t-\tau_{1,n})$ can be interpreted as the fluid velocity response to unit step voltage change. Similarly, $\Psi(t-\tau_{1,n})H(t-\tau_{1,n})$ can be interpreted as the flow rate response to unit step voltage change.

To compare the effect frequency has on the fluid velocity, two plots are generated. In first case, the frequency is set to 1Hz and in the second case it is set to 100Hz. Plots are generated for u^+=0.7mm/s, u^-=-0.3mm/s, t^+=400 ms, t^- = 600 ms, $\nu=10^{-6}$ m^2/s, h=150 μm and for u^+=0.7mm/s, u^-=-0.3mm/s, t^+=4 ms, t^- = 6 μs, $\nu=10^{-6}$ m^2/s, h=150 μm. Note that L is the time for 1 period and equals $t^+ + t^-$. The frequency is f=1/L. These parameters are selected using the geometry of the channel used for the experimental section of this thesis (see Chapter 3).

Figure 2.3 shows that the response time is nearly instantaneous for all y when the frequency is 1Hz. The velocity vs. time graphs are nearly identical for all y. With this frequency, the step changes in the voltage are so slow that they have time to propagate to the center of the channel before the next step change occurs. However, when the frequency is increased to 100 Hz (see Figure 2.4), there is significant variation in velocity vs. time graphs for different values of y. At the faster frequency, changes in the electroosmotic slip velocity do not have time to propagate through the channel. The rise time for these propagations is on the order of 10 ms.

Because the response time is so fast, the velocity profile can be approximated to be u_{slip} for all h when the frequency is below 1 Hz. This cannot be assumed when the frequency is 100 Hz.

2.2. Derivation of steady state flow rate

In this section, the flow rates generated by bipolar pulse train waveforms with various duty cycles and voltages will be compared. Because the velocity throughout the channel initially starts at zero, there are starting effects. These transients will be separated from the complete flow rate to find the steady state flow rate. This steady state flow rate allows the waveforms to be compared while neglected the starting effects.

Let $t \in [R(t^+ + t^-), (R+1)(t^+ + t^-)]$, where R is a very large, positive integer. R represents a period of the bipolar pulse train very far from the starting time. On this interval, the starting effects are negligible. By inspection, $\lim_{R\to\infty} \Psi(\mathrm{t}) = 2wh$. The flow rate can be expanded over *n* as follows:

$$Q(t) = 2u^+wh + (u^+ - u^-) * \{[\Psi(t-(t^+ + t^-))H(t-(t^+ + t^-)) - \Psi(t-(t^+ + t^-)+t^-)H(t-(t^+ + t^-)+t^-)] + \cdots + [\Psi(t-(R-1)(t^+ + t^-))H(t-(R-1)(t^+ + t^-)) - \Psi(t-(R-1)(t^+ + t^-)+t^-)H(t-(R-1)(t^+ + t^-)+t^-)] + [\Psi(t-R(t^+ + t^-))H(t-R(t^+ + t^-)) - \Psi(t-R(t^+ + t^-)+t^-)H(t-R(t^+ + t^-)+t^-)] + [\Psi(t-(R+1)(t^+ + t^-))H(t-(R+1)(t^+ + t^-)) - \Psi(t-(R+1)(t^+ + t^-)+t^-)H(t-(R+1)(t^+ + t^-)+t^-)] + \cdots\} \quad (2.10)$$

Terms that are multiplied by $H(t-\tau^*)$ where $\tau^* \geq (R+1)(t^+ + t^-)$ are dropped because they are zero for the interval considered.

$$Q(t) = 2u^+wh + (u^+ - u^-) * \{[\Psi(t-(t^+ + t^-))H(t-(t^+ + t^-)) - \Psi(t-(t^+ + t^-)+t^-)H(t-(t^+ + t^-)+t^-)] + \cdots + [\Psi(t-(R-1)(t^+ + t^-))H(t-(R-1)(t^+ + t^-)) - \Psi(t-(R-1)(t^+ + t^-)+t^-)H(t-(R-1)(t^+ + t^-)+t^-)] + [\Psi(t-R(t^+ + t^-))H(t-R(t^+ + t^-)) - \Psi(t-R(t^+ + t^-)+t^-)H(t-R(t^+ + t^-)+t^-)] + [-\Psi(t-(R+1)(t^+ + t^-)+t^-)H(t-(R+1)(t^+ + t^-)+t^-)]\} \quad (2.11)$$

Let $\bar{t} = t - R(t^+ + t^-)$. This represents the time starting at a period long after voltage is initially applied. The flow rate can by rewritten as:

$$Q(\bar{t}+R(t^{+}+t^{-}))=2u^{+}wh+(u^{+}-u^{-})*\{[\Psi(\bar{t}+(R-1)(t^{+}+t^{-}))H(\bar{t}+(R-1)(t^{+}+t^{-}))-\Psi(\bar{t}+(R-1)(t^{+}+t^{-})+t^{-})H(\bar{t}+(R-1)(t^{+}+t^{-})+t^{-})]+\cdots+[\Psi(\bar{t}+(t^{+}+t^{-}))H(\bar{t}+(t^{+}+t^{-}))-\Psi(\bar{t}+(t^{+}+t^{-})+t^{-})H(\bar{t}+(t^{+}+t^{-})+t^{-})]+[\Psi(\bar{t})H(\bar{t})-\Psi(\bar{t}+t^{-})H(\bar{t}+t^{-})]+[-\Psi(\bar{t}-t^{+})H(\bar{t}-t^{+})]\} \quad (2.12)$$

By definition, $H(t-\tau^{*})=1$ for $\tau^{*}\leq 0$, so the flow rate can be simplified as follows:

$$Q(\bar{t}+R(t^{+}+t^{-}))=2u^{+}wh+(u^{+}-u^{-})*\{[-\Psi(\bar{t}-t^{+})H(\bar{t}-t^{+})]+[\Psi(\bar{t}+(R-1)(t^{+}+t^{-}))-\Psi(\bar{t}+(R-1)(t^{+}+t^{-})+t^{-})]+\cdots+[\Psi(\bar{t}+(t^{+}+t^{-}))-\Psi(\bar{t}+(t^{+}+t^{-})+t^{-})]+[\Psi(\bar{t})-\Psi(\bar{t}+t^{-})]\} \quad (2.13)$$

When *n* is much smaller than *R*, the following limits can be defined.

$$\lim_{R\to\infty}\Psi\big(\bar{t}+(R-n)(t^{+}+t^{-})\big)=2u^{+}wh \text{ for n<<R} \quad (2.14)$$
$$\lim_{R\to\infty}\Psi(\bar{t}+(R-n)(t^{+}+t^{-})+t^{-}))=2u^{+}wh \text{ for n<<R}$$

Using these limits, the flow rate can be further simplified as:

$$Q(\bar{t}+R(t^{+}+t^{-}))=2u^{+}wh+(u^{+}-u^{-})*\{[-\Psi(\bar{t}-t^{+})H(\bar{t}-t^{+})]+[\Psi(\bar{t})-\Psi(\bar{t}+t^{-})]+[\Psi(\bar{t}+(t^{+}+t^{-}))-\Psi(\bar{t}+(t^{+}+t^{-})+t^{-})]+[\Psi(\bar{t}+2(t^{+}+t^{-}))-\Psi(\bar{t}+2(t^{+}+t^{-})+t^{-})]+\cdots\} \quad (2.15)$$

Since $Q(\bar{t})=Q\big(\bar{t}+R(t^{+}+t^{-})\big)$ for any large R, the above equation gives the steady state flow rate. Rearranging:

$$Q(\bar{t})=2u^{+}wh+\left(u^{+}-u^{-\Psi(\bar{t}-t^{+})H(\bar{t}-t^{+})}+\sum_{p=0}^{\infty}\left[\Psi\big(\bar{t}+p(t^{+}+t^{-})\big)-\Psi(\bar{t}+p(t^{+}+t^{-})+t^{-})\right]\right\} \quad (2.16)$$

The time averaged steady state flow rate is found by integrating over a full period.

$$Q_{avg}=\frac{1}{t^{+}+t^{-}}\int_{0}^{t^{+}+t^{-}}Q(\bar{t}+R(t^{+}+t^{-}))d\bar{t} \quad (2.17)$$

Evaluating this expression gives:

$$= \frac{2wh(u^+t^+ + u^-t^-)}{t^+ + t^-} + \frac{u^+ - u^-}{t^+ + t^-}\left\{\frac{4w}{h}\sum_{m=1}^{\infty}\frac{1}{\nu\beta_m^4}\left[\left(1 - e^{-\nu\beta_m^2 t^-}\right) + \sum_{p=0}^{\infty}\left(e^{-\nu\beta_m^2 p(t^+ + t^-)}\left[e^{-\nu\beta_m^2(t^+ + t^-)} + e^{-\nu\beta_m^2 t^-} - e^{-\nu\beta_m^2(t^+ + 2t^-)} - 1\right]\right)\right]\right\} \quad (2.18)$$

The flow rate is nondimensionalized and shown as follows.

$$Q\left(\bar{t}^* + R(t^{+^*} + t^{-^*})\right) = u^{+^*} + \left(u^{+^*} - u^{-^*}\right)\left\{\left[-\Psi^*\left(\bar{t}^* - t^{+^*}\right)H\left(\bar{t}^* - t^{+^*}\right)\right] + \sum_{p=0}^{\infty}\left[\Psi^*\left(\bar{t}^* + p(t^{+^*} + t^{-^*})\right) - \Psi^*\left(\bar{t}^* + p\left(t^{+^*} + t^{-^*}\right) + t^{-^*}\right)\right]\right\} \quad (2.19)$$

Where:

$$\Psi^* = \left(1 + 4\sum_{m=1}^{\infty}\frac{(-1)^m \sin(\beta_m^*)}{\beta_m^{2^*}}e^{-\nu^*\beta_m^{2^*}t^*}\right) \quad (2.20)$$

The average flow rate is nondimensionalized and shown as follows.

$$Q_{avg}^* = \left(u^{+^*}t^{+^*} + u^{-^*}t^{-^*}\right) + \frac{u^{+^*} - u^{-^*}}{t^{+^*} + t^{-^*}}\left\{4\sum_{m=1}^{\infty}\frac{1}{\nu^*\beta_m^{4^*}}\left[\left(1 - e^{-\nu^*\beta_m^{2^*}t^{-^*}}\right) + \sum_{p=0}^{\infty}\left(e^{-\nu^*\beta_m^{2^*}p(t^{+^*} + t^{-^*})}\left[e^{-\nu^*\beta_m^{2^*}(t^{+^*} + t^{-^*})} + e^{-\nu^*\beta_m^{2^*}t^{-^*}} - e^{-\nu^*\beta_m^{2^*}(t^{+^*} + 2t^{-^*})} - 1\right]\right)\right]\right\} \quad (2.21)$$

Where:

$$Q_{avg}^{*} = \frac{Q_{avg}}{2whu_{urms}} \quad , \quad u_{rms} = \sqrt{u^{+2}t^{+*} + u^{-2}t^{-*}} \quad , \quad \nu^{*} = \frac{\nu(t^{+}+t^{-})}{h^{2}} \quad ,$$
$$u^{+*} = \frac{u^{+}}{u_{rms}} \quad , \quad u^{-*} = \frac{u^{-}}{u_{rms}} \quad , \quad t^{+*} = \frac{t^{+}}{t^{+}+t^{-}} \quad , \quad t^{-*} = \frac{t^{-}}{t^{+}+t^{-}} \quad , \qquad (2.22)$$
$$\beta_{m}^{*} = \beta_{m}h$$

The flow rate appears to depend on the nondimensional term, ν^{*}. For large ν^{*}, the flow rate appears plug like, following the shape of the applied voltage exactly. The steady state and total response for large ν^{*} are also identical. However, for lower ν^{*}, there is significant rise time and a clear transient response (see Figure 2.5). Since ν^{*} represents the ratio of the length of the period to the height of the channel, shorter periods and thicker channels correspond to slower rise times. As expected, the flow velocity takes longer to reach the center of the channel in this case.

The average flow rate for various positive and negative voltage pulses are found and shown in Figure 2.6. They are plotted as a function of the ratio between the integral of the positive voltage pulse to the integral of the negative voltage pulse. The average flow rates are normalized to the root mean square of the flow rate. This normalized flow rate is effectively the flow rate produced by a DC voltage running at the root mean square of the bipolar pulse train waveform. It is assumed that the resistance of the channel is not affected by the applied voltage. Therefore the pump draws power like a simple resistor circuit where the average power is the square of the RMS voltage divided by the resistance. Since the slip velocity is linear with voltage, and the steady state flow rate with the slip velocity, taking the RMS of the flow rate allows comparison of the power usage for various waveforms.

When the areas under the positive and negative voltage pulses are equal, the average flow rate is zero for all curves because the flow produced during the positive

voltage pulse cancels out the flow produced during the negative voltage. When the duty cycle goes to 100% (V^+t^+/V^-t^- goes to infinity), the normalized flow rate approaches 1. When the duty cycle goes to 0% (V^+t^+/V^-t^- goes to 0), the normalized flow rate approaches -1. As expected, in these cases, these flow rates are identical to the flow rate produced by a DC voltage. For a given voltage pulse area ratio, a V^+ to V^- ratio of 1 uses the most power.

2.3. Movement of Particles due to Electrophoresis and Electroosmosis

The previous sections described the motion of fluid in an electroosmotic micro channel. In this section, the movement of the particles in the micro channel is considered. There are several forces acting on particles in electroosmotically driven flow: Stokes drag, the pressure force, the Basset force, and the electrophoretic force. Assuming the flow is laminar, the Basset-Boussineq-Oseen [14] equation can be used to describe the motion of the particles. This equation is shown below.

$$\frac{\pi}{6}\rho_p d_p^3 \frac{du_p}{dt} = 3\pi\mu d_p(u_f - u_p) - \frac{\pi}{6}d_p^3(\nabla p) + \frac{\pi}{12}\rho_f d_p^3 \frac{d}{dt}(u_f - u_p) + \frac{3}{2}d_p^2\sqrt{\pi\rho_f\mu}\int_{t_0}^{t}\frac{1}{\sqrt{t-\tau}}\frac{d}{d\tau}(u_f - u_p)d\tau + F_{ep}(t) \qquad (2.23)$$

This equation is a force balance for the particles. The right hand side is the mass of the particle times its acceleration. The left hand side (LHS) is the sum of the forces acting on the particle. The first term on the LHS is the Stokes drag for a spherical particle. The second term is the pressure force. The third term is the added mass term. Because the movement of the particle causes the surrounding fluid to move as well, the extra inertia of the surrounding fluid must be accounted for. The fourth term is the Basset history force. This arises because the boundary layer of the fluid has momentum and

takes time to react to the acceleration of the particles. The fifth term is the electrophoretic force [14]. The electric field used to drive the electroosmotic flow also creates a force on the particles. It is assumed to follow a repeating bipolar pulse train as discussed earlier.

The Navier-Stokes equation can be used to approximate the pressure term:

$$-\nabla p = \rho_f \frac{Du_f}{Dt} - \mu \nabla^2 u_f \tag{2.24}$$

Assuming the flow is unidirectional and fully developed, Equation 2.24 reduces to:

$$-\nabla p = \rho_f \frac{du_f}{dt} \tag{2.25}$$

Substituting Equation 2.25 into Equation 2.23, and rearranging:

$$\begin{aligned} \frac{du_p}{dt} = A\left(u_f - u_p\right) + 3B\frac{du_f}{dt} - B\frac{du_p}{dt} \\ + C\int_{t_0}^{t} \frac{1}{\sqrt{t-\tau}} \frac{d}{d\tau}\left(u_f - u_p\right)d\tau + F_{ep}(t) \end{aligned} \tag{2.26}$$

Where:

$$A = \frac{18\mu}{\rho_p d_p^2},\ B = \frac{1}{2}\frac{\rho_f}{\rho_p},\ C = \frac{9}{\sqrt{\pi}}\frac{\sqrt{\rho_f \mu}}{\rho_p d_p} \tag{2.27}$$

Here, the pressure term and the added mass terms have been combined [14]. The mass of the particle has been absorbed into F_{ep} to give f_{ep}, which represents the electric force per unit particle mass. The following equation describes f_{ep}.

$$f_{ep} = f_{ep}^{+}H(t) - \left(f_{ep}^{+} - f_{ep}^{-}\right)\sum_{n=1}^{\infty}\left(H\left(t-\tau_{1,n}\right) - H\left(t-\tau_{2,n}\right)\right) \tag{2.28}$$

f_{ep}^{+} is the electrophoretic force on the particles when the positive voltage pulse is applied and $f_{ep}^{+}$is the force when the negative voltage pulse is applied. u_p is solved for

using the Laplace transform technique [13] for solving ordinary differential equations. The result is shown below:

$$u_p = \frac{3B}{1+B}u_f + \frac{\eta}{\sqrt{\pi}}u_f * \frac{1}{\sqrt{t}} + \frac{1}{r_1 - r_2}\Big(r_1\Big((\xi + \eta r_1)u_f + f_{ep}\Big) * \Big(e^{r_1^2 t}erfc\big(-r_1\sqrt{t}\big)\Big) - r_2\Big((\xi + \eta r_2)u_f + f_{ep}\Big) * \Big(e^{r_2^2 t}erfc\big(-r_2\sqrt{t}\big)\Big)\Big) \tag{2.29}$$

Where:

$$\eta = C\sqrt{\pi}\left(\frac{1-2B}{1+B}\right),\ \xi = A\left(\frac{1-2B}{1+B}\right),\ r_1, r_2 = \frac{-C\sqrt{\pi} \pm \sqrt{C^2\pi - 4A(1+B)}}{2(1+B)}$$

$$\Phi\big(y, t-\tau_{l,n}\big)H\big(t-\tau_{l,n}\big) * \frac{1}{\sqrt{t}} =$$

$$2\sqrt{t-\tau_{l,n}} + \frac{2}{h}\sum_{m=1}^{\infty} g(y;\beta_m)\frac{-i\sqrt{\pi}e^{-\nu\beta_m^2\left(t-\tau_{l,n}\right)}\left(1-\mathrm{Erfc}\left(i\beta_m\sqrt{\left(t-\tau_{l,n}\right)\nu}\right)\right)}{\beta_m\sqrt{\nu}}$$

$$\Phi\big(y, t-\tau_{l,n}\big)H\big(t-\tau_{l,n}\big) * e^{r_k^2 t}Erfc\big(-r_k\sqrt{t}\big) =$$

$$\frac{-1-\frac{2r_k\sqrt{t-\tau_{l,n}}}{\sqrt{\pi}}+e^{r_k^2\left(t-\tau_{l,n}\right)}\left(\mathrm{Erfc}\left(-r_k\sqrt{t-\tau_{l,n}}\right)\right)}{r_k^2} + \tag{2.30}$$

$$\frac{2}{h}\sum_{m=1}^{\infty} g\big(y;\beta_m\big)\frac{-\left(\beta_m\sqrt{\nu}-ir_k+ir_k\mathrm{Erfc}\left(i\beta_m\sqrt{\left(t-\tau_{l,n}\right)\nu}\right)\right)e^{-\nu\beta_m^2\left(t-\tau_{l,n}\right)}+\beta_m\sqrt{\nu}e^{r_k^2\left(t-\tau_{l,n}\right)}\mathrm{Erfc}\left(-r_k\sqrt{t-\tau_{l,n}}\right)}{\sqrt{\nu}\beta_m\left(r_k^2+\beta_m^2\nu\right)}$$

$$H\big(t-\tau_{l,n}\big) * e^{r_k^2 t}Erfc\big(-r_k\sqrt{t}\big) = \frac{-1-\frac{2r_k\sqrt{t-\tau_{l,n}}}{\sqrt{\pi}}+e^{r_k^2(t-\tau_{l,n})}\left(\mathrm{Erfc}\left(-r_k\sqrt{t-\tau_{l,n}}\right)\right)}{r_k^2}$$

This equation describes the motion of particles in electroosmotic flow. f_{ep}^{+}, f_{ep}^{-}, u^{+}, and u^{-} remain unsolved for. u^{+} and u^{-} can be found in terms of the wall zeta potentials as shown in Section 1.2.

$$u^{\pm} = -\frac{\varepsilon\zeta_w}{\nu l}V^{\pm} \tag{2.31}$$

To find f_{ep}^{+} and f_{ep}^{-} , the fluid velocity in Equation 2.29 must first be set to zero. This leaves the electrophoretic contribution to velocity:

$$u_{ep} = \frac{1}{r_1 - r_2}\Big(r_1 f_{ep} * e^{r_1^2 t} erfc\big(-r_1\sqrt{t}\big) - r_2 f_{ep} * e^{r_2^2 t} erfc\big(-r_2\sqrt{t}\big)\Big) \tag{2.32}$$

This electrophoretic velocity can be found using the particle zeta potential as shown in Section 1.2.

$$u_{ep}^{\pm} = \frac{\varepsilon \zeta_p}{\nu l} V^{\pm} \tag{2.33}$$

These zeta potentials and must be found experimentally as will be discussed in Section 4.1.

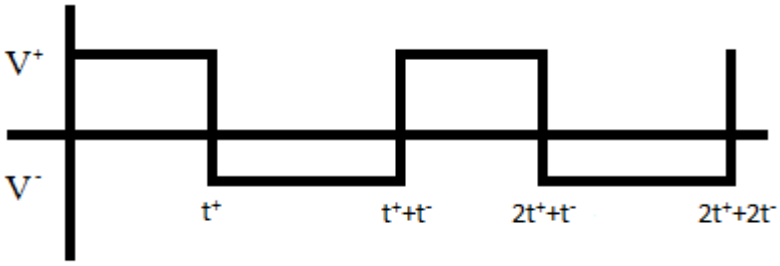

Figure 2.1. The voltage applied to the channel has the waveform above. It is a periodic function, alternating between a positive voltage pulse, V^+, for t^+ time and a negative voltage pulse, V^-, for t^- time.

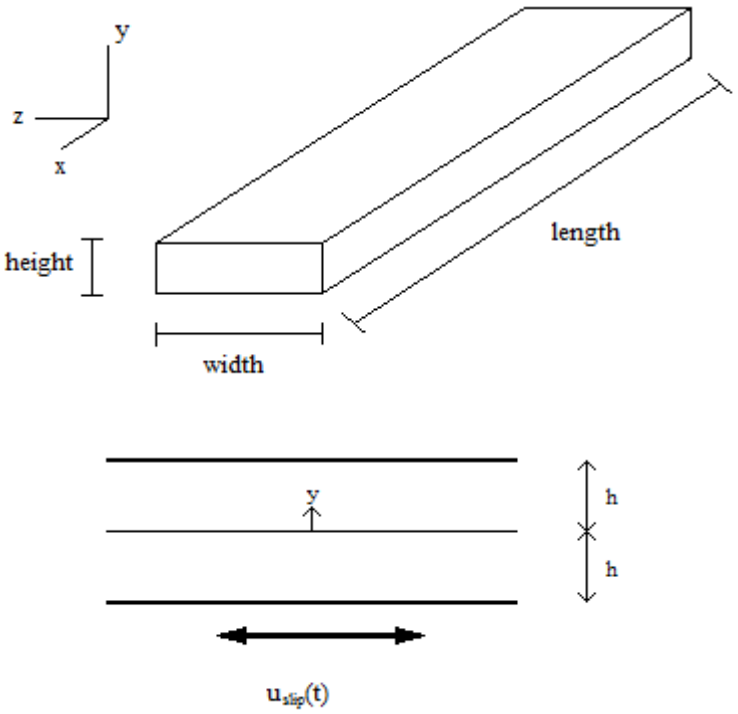

Figure 2.2. Isometric view of the channel (top). Cross-section of the channel (bottom). EO flow is approximated using a variation of Stokes' problems. The flow is assumed to be viscously dragged by the walls moving at the electroosmotic velocity, u_{slip}.

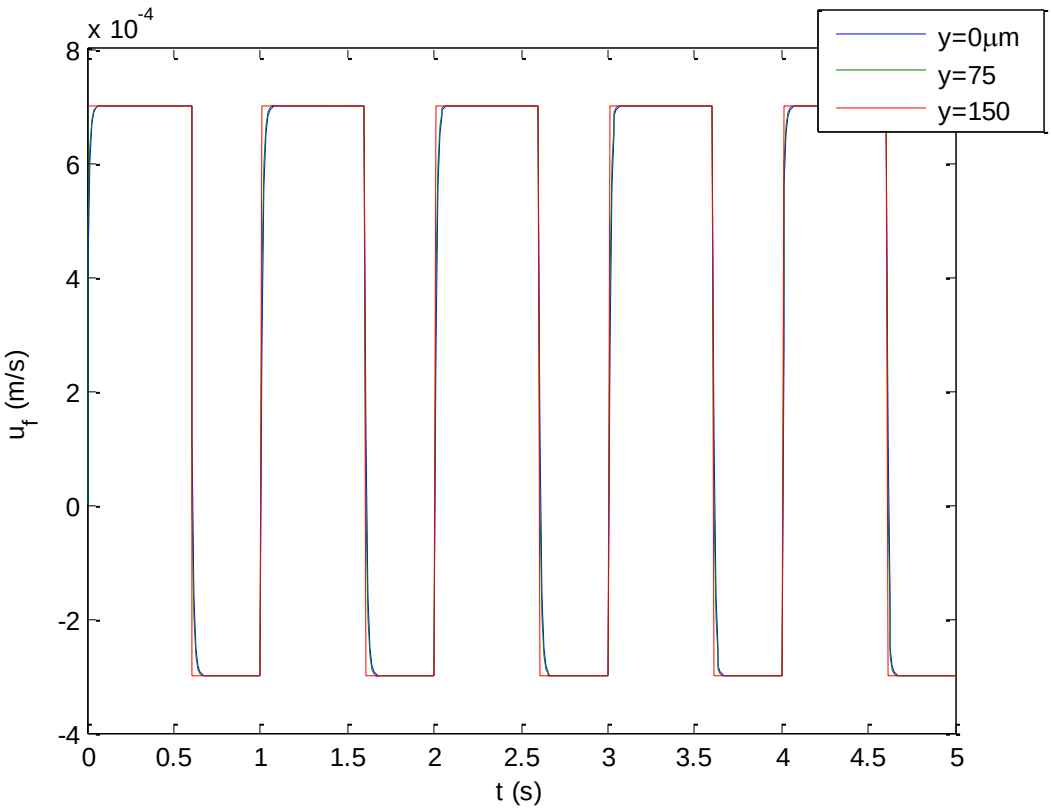

Figure 2.3. Instantaneous flow velocity, at various channel locations for an applied bipolar asymmetric waveform with f=1Hz and h=150µm. The channel height, u^+, u^-, t^+ and t^- are set to 300µm, 700µm/s, -300µm/s, 60% of period, and 40% of period. At low frequencies, there is little variation in velocity along the cross section of the channel. The velocity is approximately equal to the slip velocity everywhere in the channel.

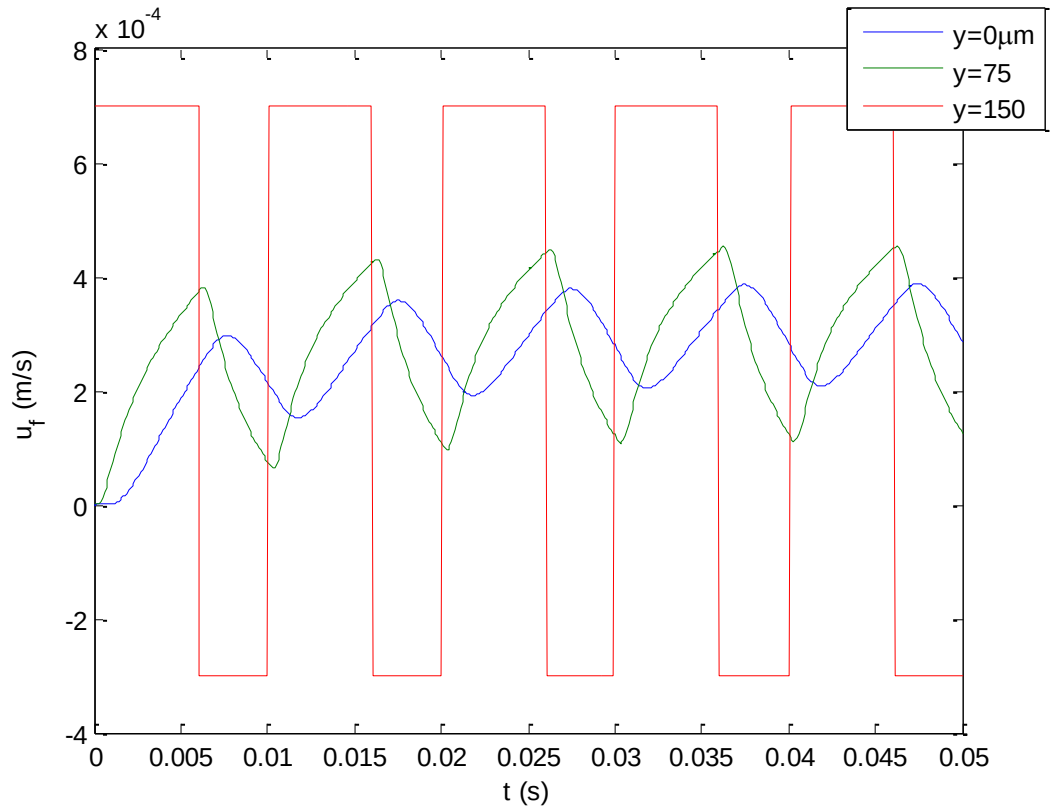

Figure 2.4. Instantaneous flow velocity, at various channel locations for an applied bipolar asymmetric waveform with f=100Hz and h=150µm. The channel height, u^+, u^-, t^+ and t^- are set to 300µm, 700µm/s, -300µm/s, 60% of period, and 40% of period. At higher frequencies, the velocities at different radial locations vary significantly. Each step change in the slip velocity does not have time to propagate throughout the channel before the next step change occurs.

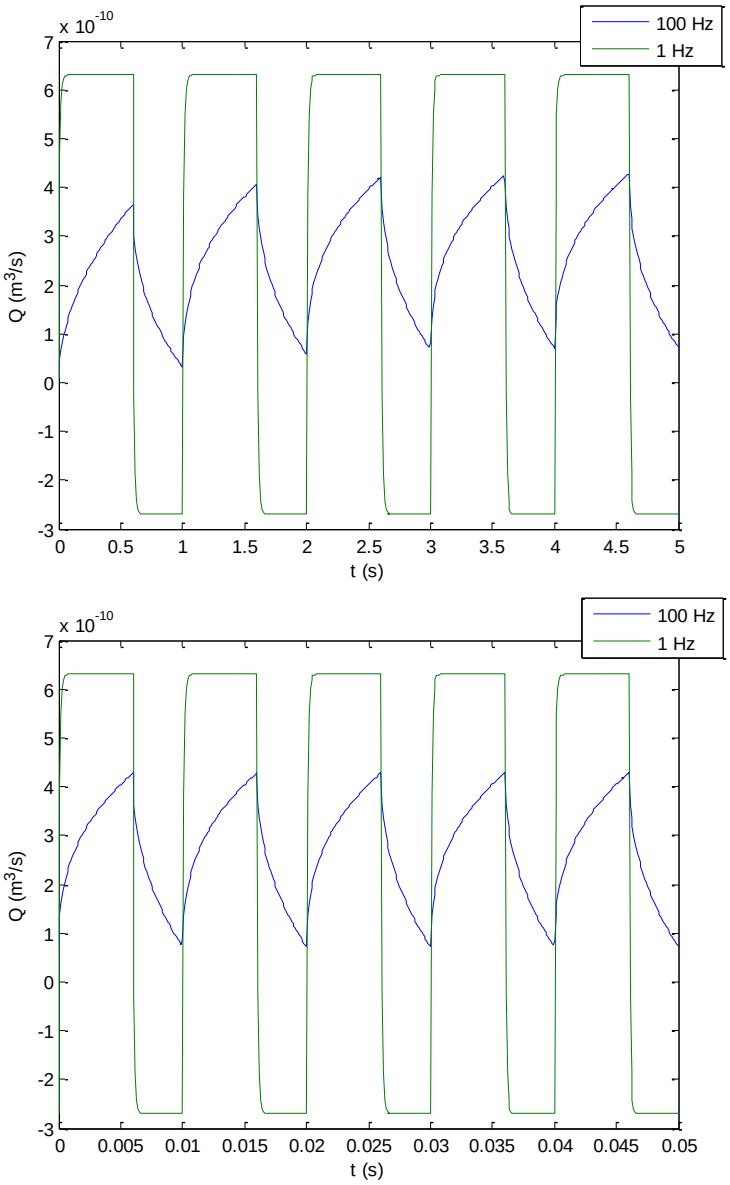

Figure 2.5. Combined steady state and transient flow rate vs. time (top). Steady state flow rate vs. time (bottom). The channel height, u^+, u^-, t^+ and t^- are set to 300µm, 700µm/s, -300µm/s, 60% of period, and 40% of period. The blue curve is for a waveform with frequency f= 1Hz ($\boldsymbol{\nu^* = 11.1}$) and the green line is for a waveform with frequency f=100Hz ($\boldsymbol{\nu^* = 0.111}$).

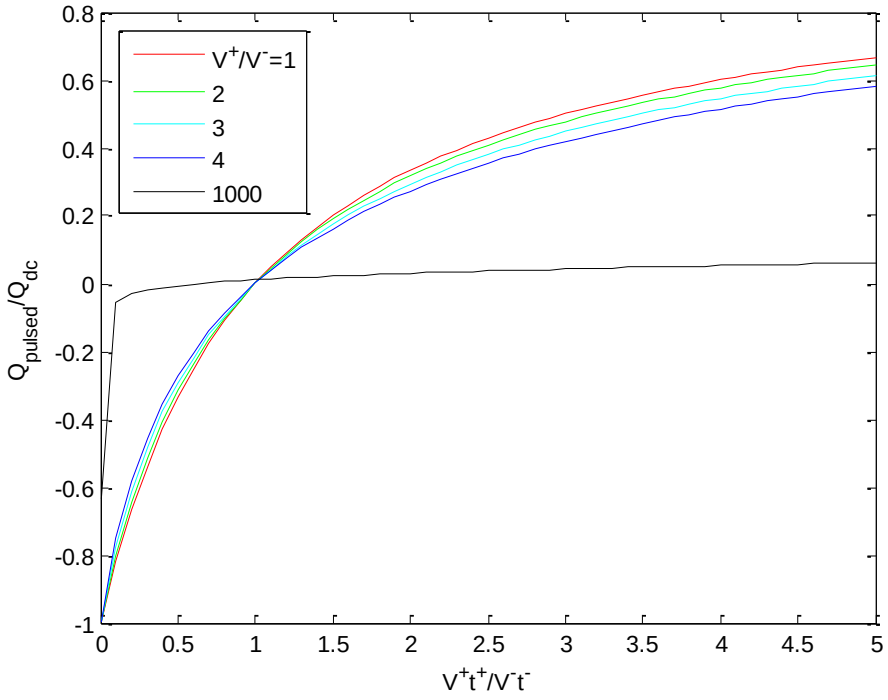

Figure 2.6. Flow rate v. ratio of the areas under the voltage curve for positive and negative voltages. Each curve represents the flow rate for different ratios of positive to negative voltage. All curves meet where the ratio of areas is one where they have zero flow rates.

Chapter 3

3.1. Manufacturing

An electroosmotic pump was designed to test the equations derived in the earlier sections. The channel height and width were chosen to be 0.3mm and 3mm. This allows the channel to be approximated as a 1D channel height wise because effects from the widthwise directions would occur at significantly slower time scale as shown in Equation 1.14. The characteristic time for electroosmotic effect in the widthwise direction is 36 seconds compared to 0.36 seconds is the height wise direction.

The pump is composed of a glass channel connecting two reservoirs. The base was constructed using three glass Fisherbrand Precleaned Microscope Slides arranged in a "U" shape. Two parallel slides were placed one centimeter apart, and the third slide was epoxied across along the bottoms of the two parallel slides. The glass channel was cut from a 0.3mm tall by 3mm wide borosilicate glass capillary tube (VitroCom VitroTubes) using a tungsten carbide glass etcher (General Scriber/Glass Etching Pen) to a length of 2cm. It was then epoxied across the gap in the base along the top.

Reservoirs were then created from a 3mL polyethylene plastic pipette from Fisher Scientific. Two, 1cm long tubes were cut from the bulb of the pipette. They were placed on either side of the glass channel so that the ends of the channel fell inside the cylinders and epoxied to the glass slides so that the bottoms of the cylinders were sealed. Figure 3.1 shows the completed electroosmotic pump.

An electrode is placed each reservoir. Inert, 0.25mm, 99.9% platinum wires from Sigma Aldrich were used to limit electrode reactions. A Tektronix AFG 3021B signal generator connected to a Trek Model 5/80 High Voltage Amplifier powers the pump.

3.2. Cleaning and Preparation

To clean the pump, first, deionized water is adding continuously to one reservoir, causing pressure to force fluid through the channel into the other reservoir, until both reservoirs are filled. The deionized water is removed and the reservoirs are refilled twice more in the same manner. The pump is connected to the power supply and a DC waveform is applied for 20 minutes. The voltage is varied until the current is around 0.5mA. This process is repeated once with a 100mM sodium hydroxide solution, once more with deionized water, and once with a 1mM borate buffer solution, with the exception of applying voltage for 40 minutes instead of 20 minutes. The 1mM borate buffer solution was chosen as the working fluid for the pump. Previous work has shown that this solution is able to produce measurable electroosmotic velocities. The 100mM NaOH cleaning solution was prepared by mixing deionized water with anhydrous sodium hydroxide. The 1mM borate buffer was prepared by mixing deionized water with anhydrous sodium tetraborate and anhydrous boric acid. All anhydrous compounds were provided by Sigma-Aldrich.

The microchannel is viewed using a Nikon Eclipse Ti-U bright field microscope with a 40X objective. Images are captured a using the high speed PowerView HS-2000 camera and the Photron FASTCAM Viewer image capture software. The camera's resolution and pixel size are 1024 x 1024 and 17μm x 17μm, giving a total field of view of 17.4mm x 17.4mm. It has an intensity range of 8 bits. The camera is mounted to the

microscope using a Nikon F-mount with 2X magnification, giving a total magnification of 80X.

0.5μm polystyrene beads (FluoSphere F8810) were used as tracer particles for these experiments. They were chosen because they appeared, on average, approximately 5 pixels in diameter on the camera, so were close to the ideal size for μPIV. These particles were received as suspensions (2% solids) in water. The suspensions were mixed with the 1mM borate buffer solution in a 10:1 solution to suspension ratio. The pump is filled with this mixture for the experiments.

3.3. Experimental Procedure

Once the particle mixture is added to the pump, the pump is mounted onto the microscope stage and connected to the power supply. The microscope is focused at the center of the channel lengthwise and widthwise and varied height wise. The bright field is switched on and the particles can be seen in through the eyepiece and the camera in Photron FASTCAM Viewer.

Two types of experiments are performed. In the first type, images are captured as DC voltage is applied to the pump. Data from this experiment can be used to calculate the electroosmotic slip velocity and the electrophoretic force as described in Chapter 2. In the second type, images are captured while a bipolar pulse train waveform, with varying positive and negative voltages and duty cycles, is applied. The camera and signal generator are synchronized via TTL so that the camera starts recording at the beginning of a period in the waveform. The signal generator is switched on a few seconds before the camera is so that the transient effects dissipate before data is gathered. The camera records at 2000 frames per second in both cases.

The captured images must be preprocessed in Matlab before they can be analyzed. First, the images are inverted so the particles show as bright spots instead of dark spots as captured in the raw images. This is required for the PIV application. Second, the images are averaged to calculate the background which is then subtracted from each image. This removes dirt and corrects for uneven lighting in the images. Finally the images are passed through a high and low pass filter. The high pass filter sharpens the images and the low pass filter reduces noise. This is achieved by separately passing the images through two Gaussian low pass filters, one with a kernel size of 31 by 31 and standard deviation of 21, and one with a kernel size of 3 by 3 and standard deviation of 3. The images from the first filter are subtracted from the images from the second filter. The images are now ready to be processed.

PIV is performed on successive image pairs using the Insight 4G PIV software using a Gaussian edge mask and an interrogation window size of 128 by 128. This results in a velocity field for each image pair. The velocity vectors are averaged for each velocity field, so each image pair gives a particle velocity for a specific time and channel height. Figure 3.2 shows a diagram of the experimental set up.

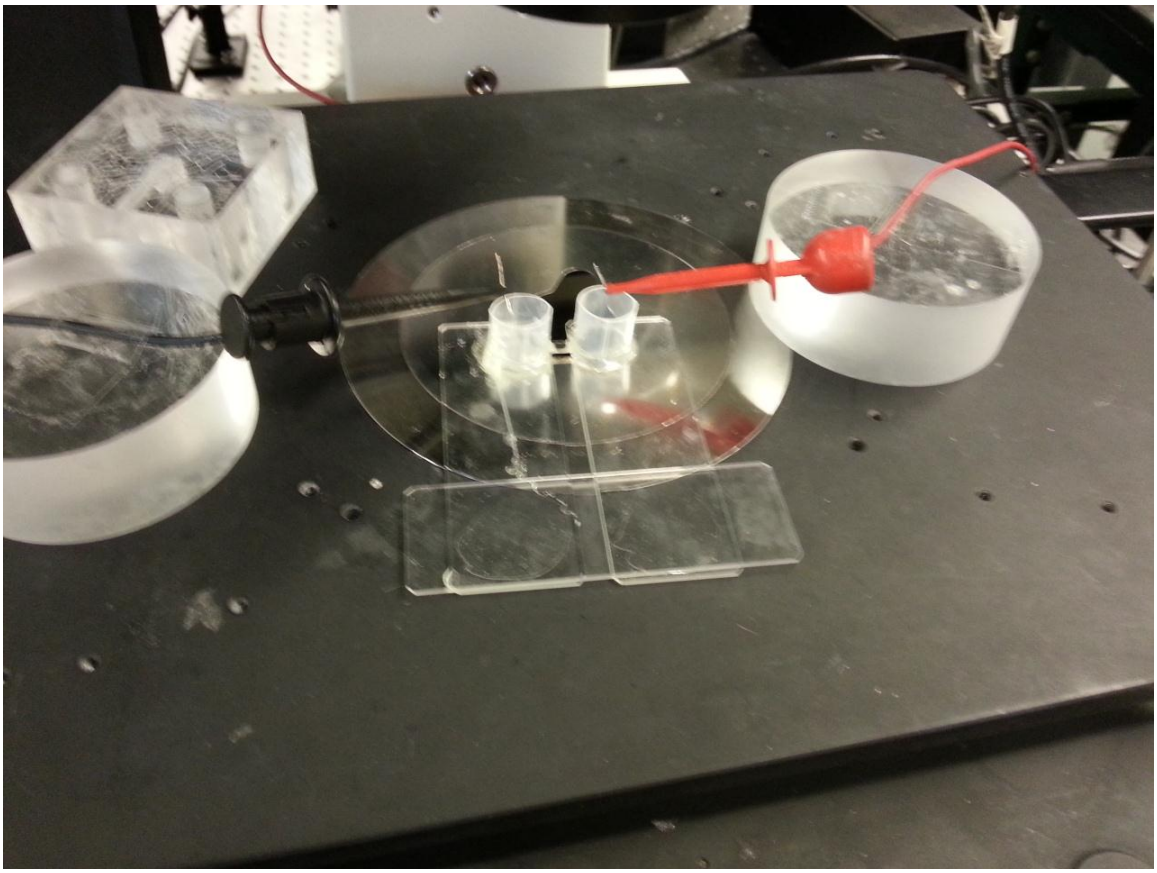

Figure 3.1. Completed electroosmotic pump used in experiments. The pump is mounted onto the microscope stage and connected to the power supply.

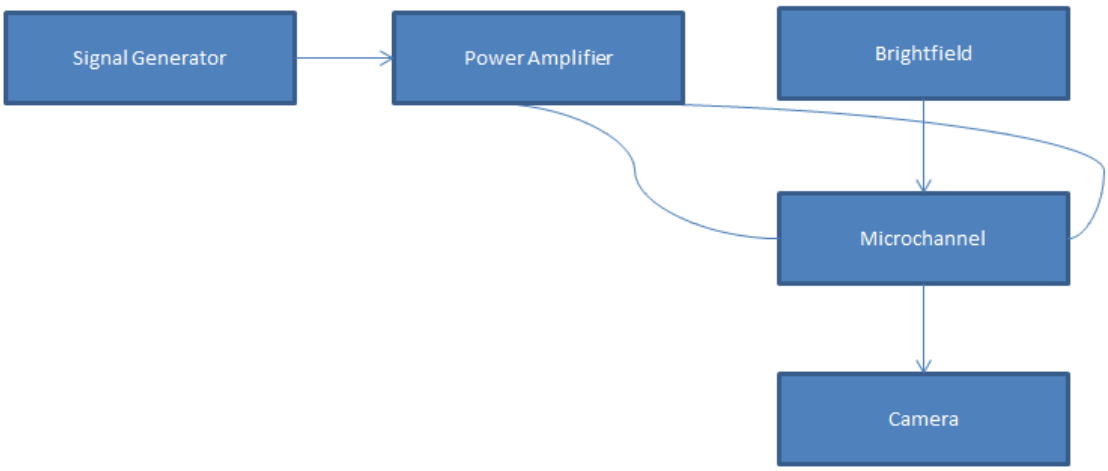

Figure 3.2. Diagram of experimental set up. The microchannel is powered by a signal generator connected to a power amplifier. The bright field illuminates the microchannel. The particle's shadows are captured by the camera and analyzed using PIV.

Chapter 4

4.1. Finding the parameters

In Section 2.3, the velocity of particles in electroosmotic flow was found in terms of the fluid velocity and the electrophoretic force. For each voltage applied to the microchannel, there are two parameters that must be solved for, the electroosmotic slip velocity and the electrophoretic force per unit particle mass. These can be found by capturing the particle velocity while voltage is applied to the channel as a step function.

Since the electroosmotic slip velocity and electrophoretic force are linear functions of voltage, the parameters for one voltage can be used to calibrate any experiment. For this analysis, V_o, u_o, and f_o will be used to designate the voltage, the associated velocity, and the associated electrophoretic force per mass. Two voltages are tested: 100V and 200V. The velocity of the particles at the center of the channel is captured as the voltage is applied, using the technique described in Section 3.3. The results are shown in Figure 4.1. From this graph, the velocity reaches a peak and then approaches a limit on the right. The peak appears because electrophoresis acts on a much shorter time scale than electroosmosis, so the particles respond quickly to the electrophoretic force. As the electroosmotic flow develops, it pushes the particles along with it.

Because the applied voltage is a step function, the step function response for electroosmosis is taken to be u_f (See Equation 2.4). The electrophoretic force is assumed to be proportional to the voltage, so a step function is also used for f_{ep}. The equations below describe u_f and f_{ep}.

$$f_{ep} = f_o H(t) \qquad (3.1)$$

$$u_f = u_o \Phi(\mathrm{y} = 0, \mathrm{t}) \qquad (3.2)$$

Equations 3.1 and 3.32 are substituted into particle velocity equation (see Equation 2.29). f_o and u_o are varied until the peak and right side limit shown match the experimental data. The results of the matching are shown in Figure 4.1. For comparison, the theoretical particle velocity was calculated, ignoring the added mass. This result differs from the full solution to the B-B-O equation. The Basset force appears to have a much smaller effect. When it is cancelled, the calculated velocities do not differ from the full solution to the B-B-O equation. u_o and f_o were found to be -183μm/s and 3.47 x 10^6 m/s^2, respectively for 100V; and -380μm/s and 7.50 x 10^6 m/s^2, respectively for 200V.

As expected, the electrophoretic force and electroosmotic slip velocity for 200V is roughly double the values for the 100V case. The electroosmotic slip velocity for this channel configuration is 3.73 x 10^{-4} cm^2/V-s. The particle charge can also be found using Coulomb's Law:

$$F_{ep} = f_{ep} m_p = q_p E \qquad (3.3)$$

The charge of the particles is 4.96 x 10^{17} C. Since u_o and f_o are known for an applied voltage of 100V and 200V, the velocity of the particles can be found for when a repeating bipolar pulse train is applied. The square wave response for electroosmosis is taken to be u_f (See Equation 2.6). Since the electrophoretic force is proportional to the voltage, a square wave can also be used for f_{ep}. Equation 2.29 now fully describes the velocity of the particles with all the parameters known.

4.2. Particle velocity due to bipolar pulse train voltage

The time resolved velocity distribution of the particles in response to the repeating bipolar pulse train voltage is captured using PIV. Data is captured along channel height for two waveforms.

The particle velocity in response to a square waveform is first captured. (V^+ = 100V, V^- = -100V, $t^+ = t^-$ = 0.005s). Using Equation 2.29 with the parameters found in the previous section, the theoretical particle velocity distribution can be found.

The measured velocity profiles and calculated velocity profiles are compared in Figure 4.2 and 4.3. In Figure 4.2 the particle velocity profiles are shown and in Figure 4.3 the fluid velocity profiles are shown. These are taken at various times spanning across a full period of the voltage waveform from the center of the channel to the top wall. t=0 and t=0.005s mark the transition from the negative to positive voltage pulse and the positive to negative voltage pulse, respectively. Away from these transitions, the velocity profiles match closely. However, at these transitions, the velocity profiles significantly differ. This error likely occurs because of the limited frame rate of the camera. Because voltage is discontinuous at these times, the velocity changes too quickly, and the camera cannot capture the profile correctly.

The particle velocity as a function of time at various channel heights is next compared in Figure 4.3. Here, the measured and calculated values match somewhat closely. The experimental data match the theory very well when y=0 and y=75μm. At the wall, however, there is significant error. Due to the scarcity of particles near the wall and light scattering due to the wall [], data had to be captured some distance away from the wall. The experimental fluid velocity can be calculated by subtracting the electrophoretic effect from the experimental particle velocity. From Equation 2.9, the electrophoretic part

of the particle velocity can be found by ignoring the electroosmotic terms. This results in the following equation.

$$u_{ep} = \frac{1}{r_1 - r_2}\Big(r_1 f_{ep} * e^{r_1^2 t} erfc\big(-r_1\sqrt{t}\big) - r_2 f_{ep} * e^{r_2^2 t} erfc\big(-r_2\sqrt{t}\big)\Big) \quad (3.4)$$

This electrophoretic velocity is subtracted from the particle velocity to give the experimental fluid velocity. The experimental fluid velocity is compared to the theoretical fluid velocity in Figure 4.4. The velocities are similar everywhere except at the voltage pulse transitions. Again, the discontinuity in voltage cannot be captured by the cameras because the frame rate is limited.

The flow rate was then calculated and compared in Figures 4.5 and 4.6 for two different waveforms. In Figure 4.5, the voltage was applied as a square wave with a peak to peak voltage of 200V and frequency of 100Hz. The experimental and theoretical flow rates match very closely, except at the voltage transitions. As described earlier, this is due to the limited frame rate of the camera. In Figure 4.6, voltage is applied as a bipolar pulse train with V^+ = 200V, V^- = -100V, 100 Hz frequency, and 25% duty cycle. Here, the experimental and theoretical plots look similar initially, but at the voltage transition, the flow rates deviate. This is likely due to back pressure building up in the reservoirs. Because the average flow rate in this case is nonzero, pressure builds up in one reservoir to oppose the electroosmotic flow.

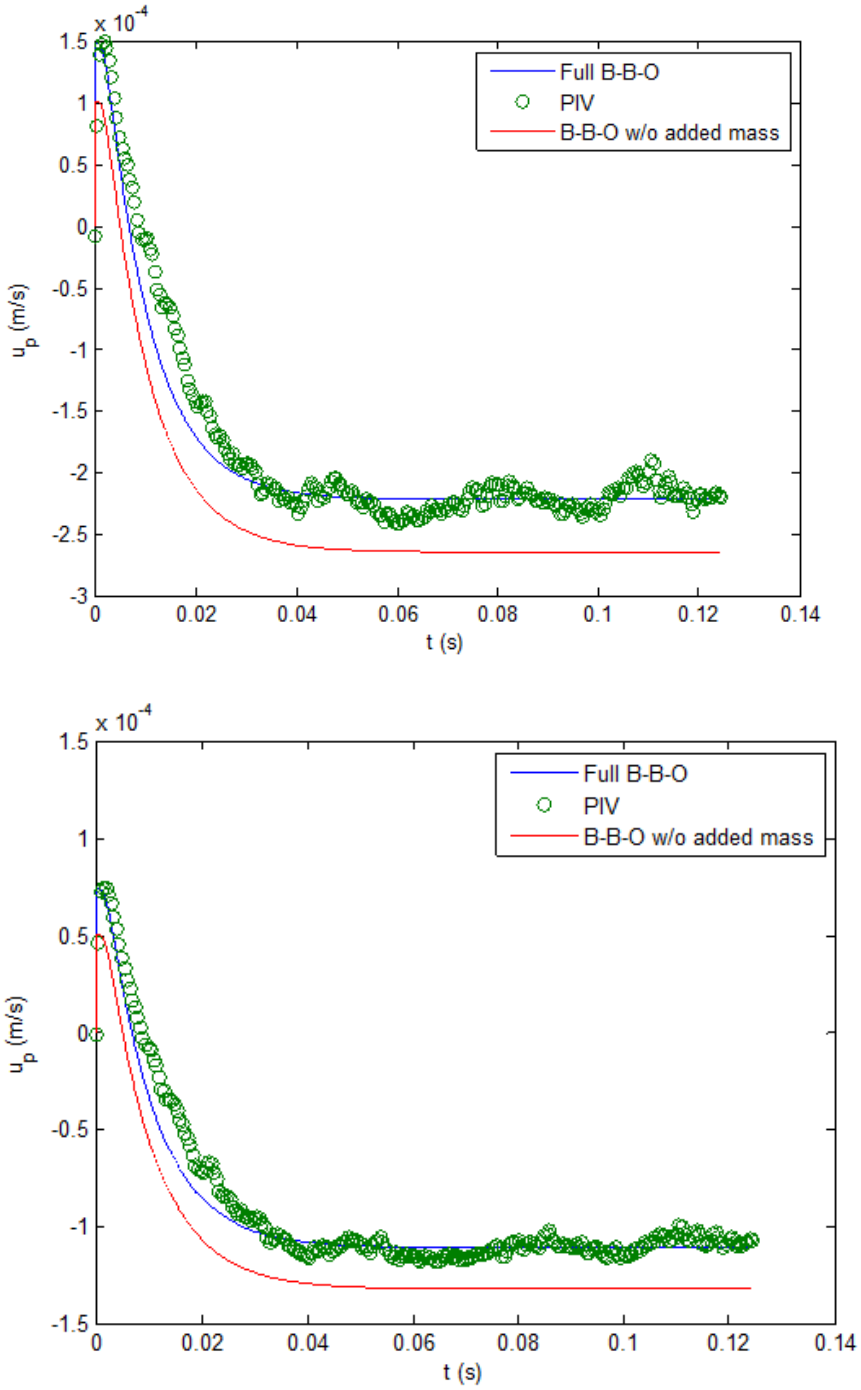

Figure 4.1. Particle velocity due to a 100V (top) and 200V (bottom) step waveform. The blue graph is found using high speed PIV. The green graph is found be solving the Basset–Boussinesq–Oseen equation and matching the peak and right side limit with the blue graph. The red graph shows the theoretical particle velocity ignoring the added mass term.

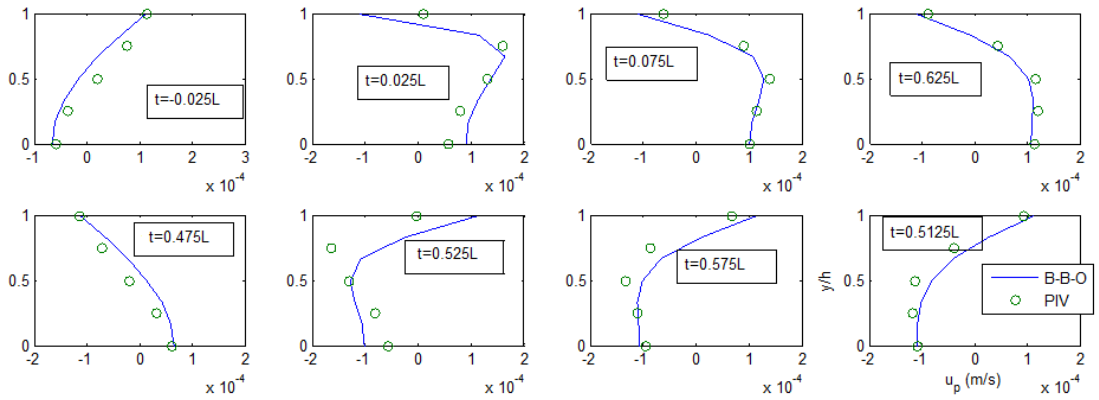

Figure 4.2. Selected particle velocity profiles. The top side shows the velocity profiles at a negative to positive slip velocity transition, starting from the center of the channel to the edge of the channel. The left side shows the velocity profiles at a positive to negative velocity transition, starting from the center of the channel to the edge of the channel. These plots show the top half of the velocity profiles and are for 300μm high rectangular channel, using a square wave of 200V peak to peak at 100Hz.

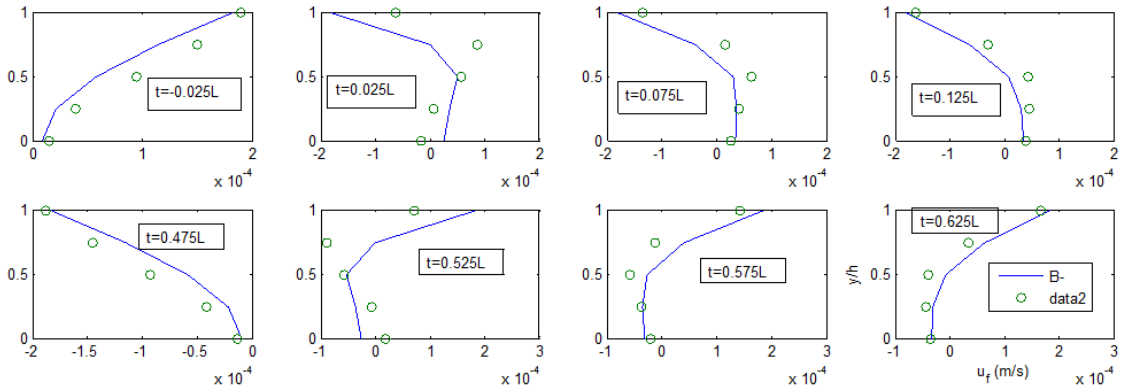

Figure 4.3. Selected fluid velocity profiles. The top side shows the velocity profiles at a negative to positive slip velocity transition, starting from the center of the channel to the edge of the channel. The left side shows the velocity profiles at a positive to negative velocity transition, starting from the center of the channel to the edge of the channel. These plots show the top half of the velocity profiles and are for 300μm high rectangular channel, using a square wave of 200V peak to peak at 100Hz.

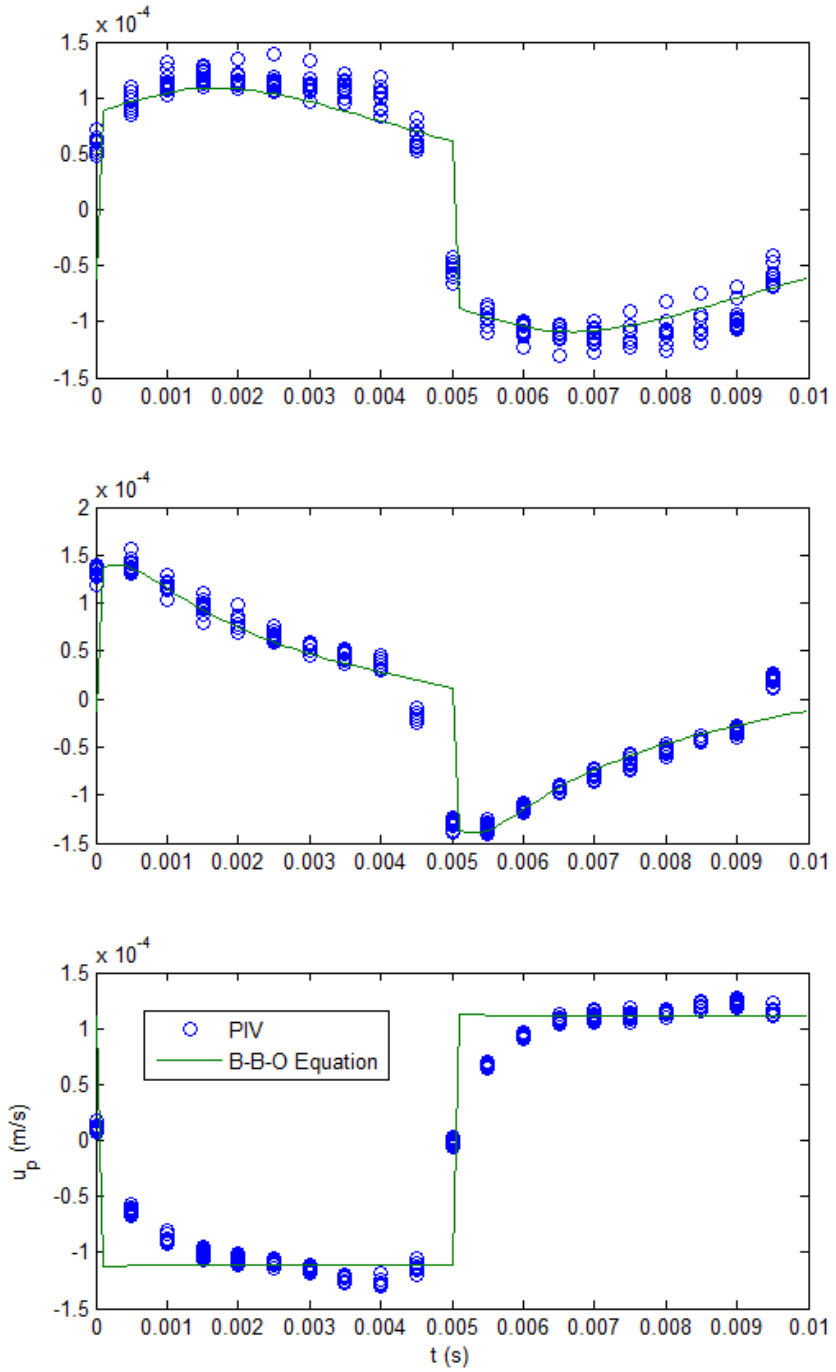

Figure 4.4. Particle velocity due to a 200$V_{p\text{-}p}$, 100Hz square waveform at the channel heights: y=0 (top), y=75µm (middle), and y=150 µm (bottom). The green graph is found using high speed PIV. The blue graph is found by solving the Basset–Boussinesq–Oseen equation.

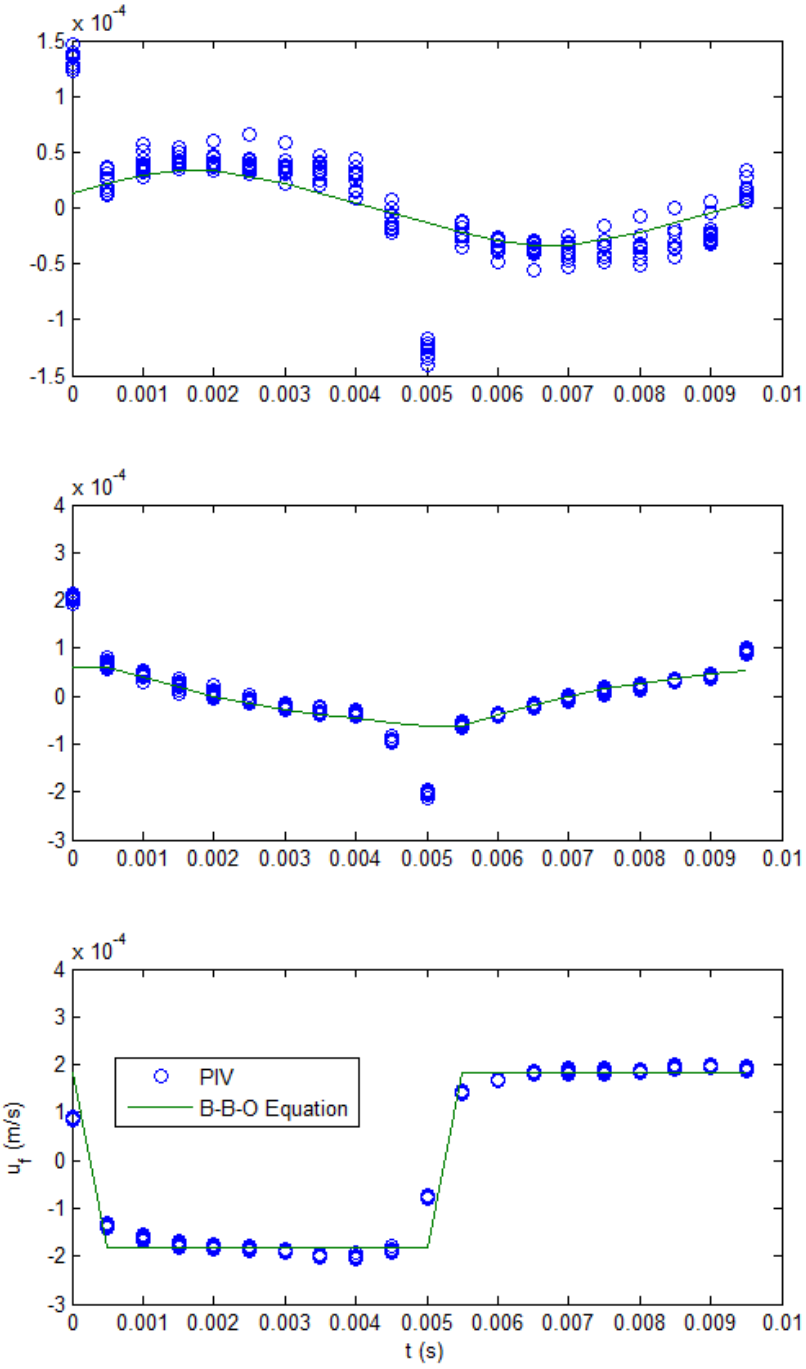

Figure 4.5. Fluid velocity due to a 200$V_{p\text{-}p}$, 100Hz square waveform at the channel heights: y=0 (top), y=75µm (middle), and y=150 µm (bottom). The green graph is found using high speed PIV. The blue graph is found by solving the Basset–Boussinesq–Oseen equation

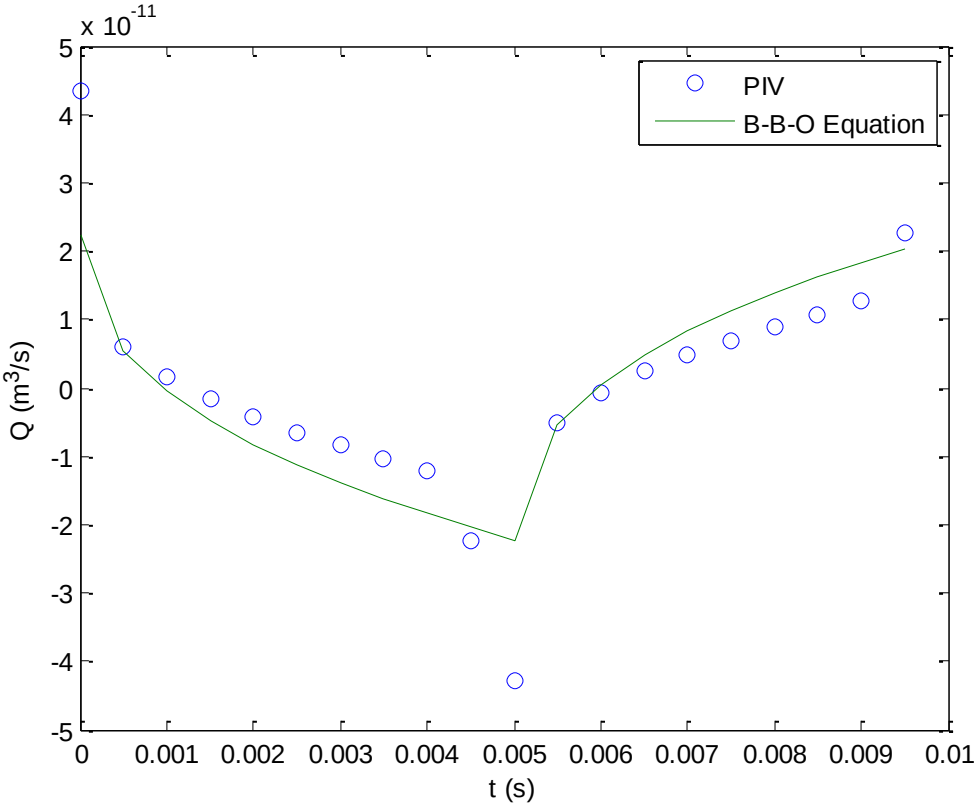

Figure 4.6. Comparison of flow rate vs. time obtained experimental, with PIV and theoretically, with the Basset-Boussinesq-Oseen equation. Multiple periods were captured with PIV and averaged. A $200V_{p\text{-}p}$ square wave with a 100Hz frequency was applied to the pump.

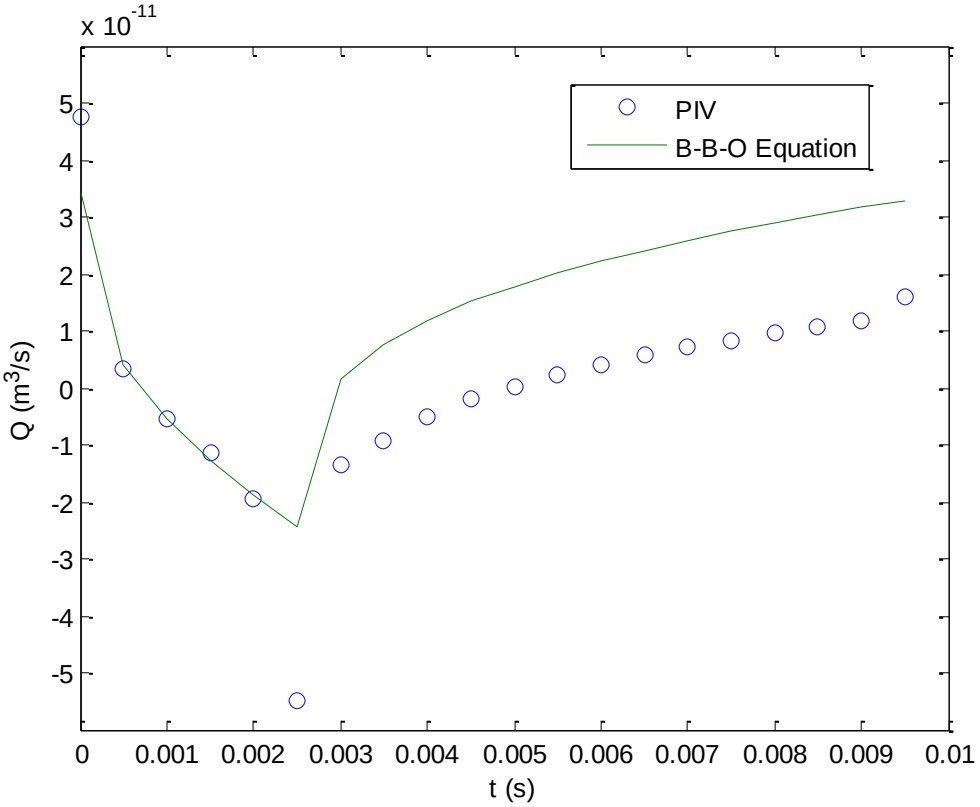

Figure 4.7. Comparison of flow rate vs. time obtained experimental, with PIV and theoretically, with the Basset-Boussinesq-Oseen equation. Multiple periods were captured with PIV and averaged. A pulse train with a 100Hz frequency, $V^+ = 200V$, $V^- = -100V$, and 25% duty cycle was applied to the pump.

Conclusion

The experimental and theoretical particle and fluid velocity obtained in this thesis show good agreement. The fluid and particle velocity distributions match very well for towards the center of the wall and away from the voltage pulse transitions. Using the techniques described, the electrophoretic force, particle charge, and electroosmotic mobility were also found.

Errors were mainly caused by limitations in the camera. During the voltage transitions, camera frame rate was too low to accurately capture the particle velocity. A camera with a higher frame rate can be used, in the future, to measure the velocity distributions during the transitions. Another issue was the effect of back pressure on the fluid velocity. The pressure build up in the reservoirs can be accounted for in the electroosmotic velocity distribution. The fluid and particle velocity for non-net zero average flow rates can then be compared. The parameters and dimensions used for the experiments can also be varied to further test the equations presented in this thesis. For example, the channel height, particle size, and particle density can all be varied.

References

1. P. Abgrall and A.-M. Gue, “Lab-on-chip technologies: making a microfluidic network and coupling it into a complete microsystem—a review.” *J. Micromech. Microeng.*, 2007, Vol. 17. R15-R49.

2. B. J. Kirby, *Micro- and Nanoscale Fluid Mechanics: Transport in Microfluidic Devices.* New York : Cambridge UP, 2010.

3. V. S. Bagotsky, *Fundamentals of Electrochemistry.* New York : Wiley-Interscience, 2011. 2nd ed.

4. H.-C. Chang and L. Y. Yeo, *Electrokinetically-Driven Microfluidics and Nanofluidics.* New York : Cambridge UP, 508. 1st ed.

5. N.-T. Nguyen and S. T. Wereley, *Fundamentals and Applications of Microfluidics.* Norwood, MA : Artech House, 2006. 2nd ed.

6. M. Minor, et al, “Dynamic Aspects of Electrophoresis and Electroosmosis: A New Fast Method for Measuring Particle Mobilities.” *J. Colloid Interface Sci.*, 1997, Vol. 189. 370-375.

7. M. Sureda, A. Miller, and F. J. Diez, “In situ particle zeta potential evaluation in electroosmotic flows from time-resolved microPIV measurements.” *Electrophoresis*, 2012, Vol. 33. 2759-2768.

8. D. Yan, C. Y. Nguyen, and Huang, X, “Visualizing the transient electroosmotic flow and measuring the zeta.” *J. Chem. Phys.*, 2005, Vol. 124. 370–375.

9. S. N. Smirnov, “Electric Double Layer.” *New Mexico State University.* [Online] [Cited: June 21, 2013.] http://web.nmsu.edu/~snsm.

10. P. Dutta and A. Beskok, “Analytical Solution of Time Periodic.*” Anal. Chem.*, 2001, Vol. 73. 5097-5102.

11. P. K. Kundu, I. M. Cohen, and D. R. Dowling, David R. *Fluid Mechanics.* New York : Academic Press, 2011. 5th ed.

12. I. M. Ozisik, *Heat Conduction.* New York : Wiley, 1993. 2nd ed.

13. D. G. Zill and W. S. Wright, *Advanced Engineering Mathematics.* Sadbury, MA : Jones & Bartlett Publishers, 2009. 4th ed.

14. C. T. Crowe, M. Sommerfeld, and Y. Tsuji, *Multiphase Flows with Droplets and Particles Flows.* Boca Raton, FL : CRC Press, 1997.